communications earth & environment

Article

https://doi.org/10.1038/s43247-024-01830-9

Habitat suitability models reveal extensive distribution of deep warm-water coral frameworks in the Red Sea

Megan K. B. Nolan [1,2] ✉, Fabio Marchese[1], Sam J. Purkis [3], Mustapha Ouhssain[1], Malika Kheireddine[1], Tullia I. Terraneo[1], Giovanni Chimienti[4], Mattie Rodrigue[5], Ameer A. Eweida[6], Burton Jones [1,2] & Francesca Benzoni [1,2]

Deep-sea coral frameworks are understudied in the Red Sea, where conditions in the deep are conspicuously warm and saline compared to other basins. Habitat suitability models can be used to predict the distribution pattern of species or assemblages where direct observation is difficult. Here we show how coral frameworks, built by species within the families Caryophylliidae and Dendrophylliidae, are distributed between water depths of 150 m and 700 m in the northern Red Sea and Gulf of Aqaba. To extrapolate the known (ground-truthed) positions of these deep frameworks, we use environmental and geomorphometric variables to inform well-performing maximum entropy models. Over 250 km^2 of seafloor in our study area are identified as suitable for such frameworks, equivalent to at least 35% of the area of photic-zone coral reefs in the same region. We hence contend that deep-water coral frameworks are an important and underappreciated repository of Red Sea biodiversity.

Global climate change and the increase of anthropogenic impacts on our natural environments mean that conservation is now more important than ever[1], and it is vital that management efforts are focused in the most suitable areas. For maximum efficiency, conservation planning requires detailed knowledge of local biodiversity and its spatial distribution[2], yet these data are often lacking due to difficulties in accessing the area, or limited funding for baseline studies. Such deficits are particularly acute for marine environments, and marine spatial planning projects are often restricted by extent or depth due to a lack of data[3]. Shallow coral reefs are one of the most biodiverse ecosystems[4], supporting people globally through a host of ecosystem services, including provisioning of food for local communities, coastal protection and tourism[5–7]. To conserve the biodiversity and ecosystem services of reefs, it is necessary to understand their global distribution. In the case of shallow coral reefs, satellite imagery can be used to map the locations of many habitats[8–12]. However, satellites have a practical depth limit of around 30 m, even in ideal conditions, set by the physics of light in water[13]. This depth is also the approximate limit for safe SCUBA diving, hampering the collection of ground-truth observations with which to calibrate the satellite observations and assess accuracy. So obscured from casual view, the distribution of deeper reefs is poorly documented[14–16].

Deep coral ecosystems are found below the mesophotic zone, deeper than 150 m water depth[17], and convey many of the same ecosystem services as shallower coral reef ecosystems, such as providing habitat for fish, promoting biodiversity and increasing secondary production[18–20]. Non-destructive techniques to study deep ecosystems generally rely on expensive technologies, such as remotely operated vehicles (ROVs) and submersibles (subs)[21]. Studies of deep coral assemblages are therefore focused on just a few areas, for example, the northern Atlantic[16,18,22–24], southern Atlantic[15,25], and Mediterranean Sea[18,26–29]. Despite deep reefs appearing to be far from human pressures, they are in fact gravely threatened[30], particularly due to global warming[31] and ocean acidification[32,33]. Other threats are more localised and visible, such as anthropogenic litter[34] and trawling[35,36]. It is hence important to understand the composition and extent of these habitats, in order to establish a baseline assessment against which future impacts, and, hopefully recovery, might be assessed.

Globally, deep coral ecosystems are formed by cold-water corals[35,36] commonly between 150 and 2000 m deep[25,37,38], with depth records from over 6000 m deep[39]. Typically, deep, cold-water corals are found to live in areas with temperatures of 4–13 °C and salinities of 32–39 ppt[35,36]. However, unusually warm-water temperatures at depth in the Red Sea (above 20 °C at over 2000 m depth[40,41]) indicate the unique presence of deep, warm-water

[1]Red Sea Research Center, King Abdullah University of Science and Technology, Thuwal, Saudi Arabia. [2]Marine Science Program, King Abdullah University of Science and Technology, Thuwal, Saudi Arabia. [3]Department of Marine Geosciences, Rosenstiel School of Marine, Atmospheric and Earth Science, University of Miami, Miami, FL, USA. [4]Department of Biosciences, Biotechnologies and Environment, University of Bari Aldo Moro, Bari, Italy. [5]OceanX, New York, NY, USA. [6]NEOM, Riyadh, Kingdom of Saudi Arabia. ✉e-mail: megan.nolan@kaust.edu.sa

corals[42]. The ecology and physiology of these corals, which have evolved and adapted to these unique environmental conditions, are poorly understood. Since the presence of deep, warm-water corals was first recorded in the Red Sea by Marenzeller[43], only relatively small-scale surveys for corals have been conducted in this region[40,44–46], and no systematic surveys have been completed. More recently, frameworks built by a single coral, *Eguchipsammia fistula* (Alcock, 1902) (Scleractinia, Dendrophylliidae), were described at 640 m depth, first identifying these habitats in the Red Sea[44]. Frameworks are complex 3D coral-dominated areas with sufficient topographic relief to modulate the shape of the seafloor. Living frameworks are typically surrounded by substantial accumulations of coral rubble, resulting from the breakdown of the structure[47]. When coral frameworks form in shallow water, there are a myriad of carbonate-secreting organisms that act to bind the framework, such as crustose coralline algae (CCA) and encrusting bryozoans[48]. These 'binders' aid the corals in forming dense rigid reef frameworks[49]. However, many of these known binders do not occur in the aphotic conditions of the deep sea (some exceptions include serpulids and sponges), and deep frameworks are, therefore, less robust than their shallow counterparts. In addition to the dead coral framework that plays an important role in maintaining the positive relief structure, the resultant production of coral rubble has been shown to increase metabolic activity and resource cycling[50], and serves as a settlement substrate for other benthic and meiofaunal organisms, such as nematodes, lace corals and sponges[18,23,51–53]. For these reasons, deep reefs create abundant habitat and promote biodiversity.

To further assess the distribution of deep, warm-water coral frameworks in the Red Sea, we need more information about their location and composition[54,55]. Whereas it is unfeasible to manually collect such observational data at scale, it is possible to extrapolate the sparse existing data using predictive models. One example is habitat suitability models (HSMs; e.g., ref. 56), which combine verified presence observations with continuous layers of environmental or physical variables, in order to estimate the areas which may be suitable for the species or assemblage of interest[57]. Such models have been used extensively across terrestrial[58,59] and marine environments and in shallow[7,60,61] and deep waters[62,63]. One common method uses a maximum entropy algorithm, which aims to provide a distribution of suitable habitats as uniformly as possible for the given data[64,65]. As well as being one of the most popular tools[66], it has also been shown to be one of the best-performing algorithms for habitat suitability models[67–70].

Here, we show the most suitable distribution of deep-water coral framework in the Red Sea, as formed by four different coral species—*Eguchipsammia fistula*, *Dendrophyllia* cf *cornigera* (Lamarck, 1816) *sensu* Scheer and Pillai[71] *Caryophyllia* sp. and *Rhizosmilia valida* (Marenzeller, 1907). Based on recent explorations conducted aboard a research cruise facilitated by OceanX, we present the first spatial models of a coral framework in the deep Red Sea. We compare our model predictions for the distribution of deep-water corals in the northern Red Sea and Gulf of Aqaba with the verified distribution of shallow-water corals in the same area[61,72]. We contend that our predictions on the distribution and composition of the deep-water coral systems will aid conservation planning along the rapidly urbanising Saudi Arabian Red Sea coastline.

Results

We identified the presence of deep, warm-water coral framework in 20 ROV and sub-dives from the 63 that were conducted between 150 and 700 m (Fig. 1a, b). All of these presences were north of the framework reported by Qurban et al.[44]. Based on both videos and collected samples, we were able to identify two different types of framework, built by corals of one of two families, Caryophylliidae or Dendrophylliidae. We have named these two framework types Caryophylliidae Coral Framework (CCF) and Dendrophylliidae Coral Framework (DCF), respectively. The frameworks differed in their depth distribution, CCF was found between 300 and 700 m, while DCF was identified from 150–500 m depth. CCF was built by *Rhizosmilia valida*, or a second, as yet undescribed, species (*Caryophyllia* sp.), while DCF was built by *Eguchipsammia fistula* or *Dendrophyllia* cf *cornigera* (Figs. 2 and Fig. 3).

We used MaxEnt (v.3.4.4) to generate maximum entropy habitat suitability models for two coral assemblages from environmental and geomorphometric predictor variables (Table 1). A stepwise selection process (see 'Methods') was used to generate the best-performing models, assessed using the AUC (Area Under the receiver operating characteristics Curve) and the TSS (True Skill Statistic: see methods for further explanations) value based on the 30% data withheld for testing. No variables were strongly correlated, as all had an r2 value below 0.7 (Fig. 4). For each assemblage, the final best-performing model contained many of the initial variables (described below), highlighting the common understanding that a stricter set of predictor variables often does not improve the output of models produced with MaxEnt[64,67,73].

Model validation

The AUC value for the final models, based on test data, was high: 0.987 and 0.990 for CCF and DCF, respectively. When we further controlled for spatial autocorrelation, the average AUC was comparable, remaining high, at 0.987 and 0.961 for CCF and DCF (Table S1), indicating that this was not a large issue in our initial study design. In all cases, the AUC was above 0.8; an AUC above 0.5 represents a better-than-random chance of accurate results, whereas 0.7 is often considered a threshold for defining a good and reliable model. Our results remain well above this and, therefore, indicate robust, well-performing models. Furthermore, the calculated TSS was, on average, 0.927 for CCF and 0.943 for DCF (Table S2). In all cases, this statistic was above 0.88, supporting the AUC values and providing further confidence in our results.

Opportunistic and independent data collection occurred during the Red Sea Relationship Cultivation mission, on board M/V OceanXplorer in 2022, using the same equipment as the Deep Blue expedition of 2020. From this, we were able to use completely independent data to assess model performances. During this expedition, both CCF and DCF were identified in five independent ROV/sub-dives. Many of these dives returned to known areas of framework, so were not considered here as they are not spatially independent. This resulted in three sub-dives, in two separate locations where CCF was newly observed, and one sub-dive during which a previously unknown area of DCF was observed. One area of CCF (transects NTN0180 and NDR0927) was identified as highly suitable by our models, while the other area (transect NTN0182) was not identified as highly suitable, but located close to an area which was (Fig. S1). The new area of DCF (dive NTN0182) was identified as being moderately suitable by our model, with suitability mostly between 0.5 and 0.75. While the sample size is relatively low, the inclusion of these additional validation points allows greater confidence in the models. Furthermore, Qurban et al.[45], reported an area in which a framework resembling CCF was identified. While we do not know the exact area in which this framework was found, it overlaps with the considerable area identified by our models as highly suitable, providing independent ground-truthed validation.

Due to some doubts in the literature about the weight given to the AUC in validating models[74], we calculated the average errors of omission and commission from the opportunistic ground-truth data. The error of omission represents the proportion of the data where the habitat is incorrectly identified as unsuitable (false negative) and is used to calculate the user's accuracy[75]. The error of commission is the portion of the data where the habitat is incorrectly identified as suitable (false positive) and is used to determine the producer's accuracy[75]. From this, we calculated the overall accuracies for each model; this was 85.7% for CCF and 82.6% for DCF (Table 2). The high accuracy values indicate low error values in our results. However, a larger sample size for external validation would have provided additional confidence in the AUC values reported above.

Caryophylliidae Coral Framework (CCF)

Caryophylliidae Coral Framework (CCF) was reported from 14 dives in the northern Red Sea. The highest density was seen in the south of NEOM Bay, northwest of Duba Seaport (Fig. 5c). The assemblage was also identified in two locations just south of Sanafir Island, as well as northwest of Tiran Island (Fig. 5b).

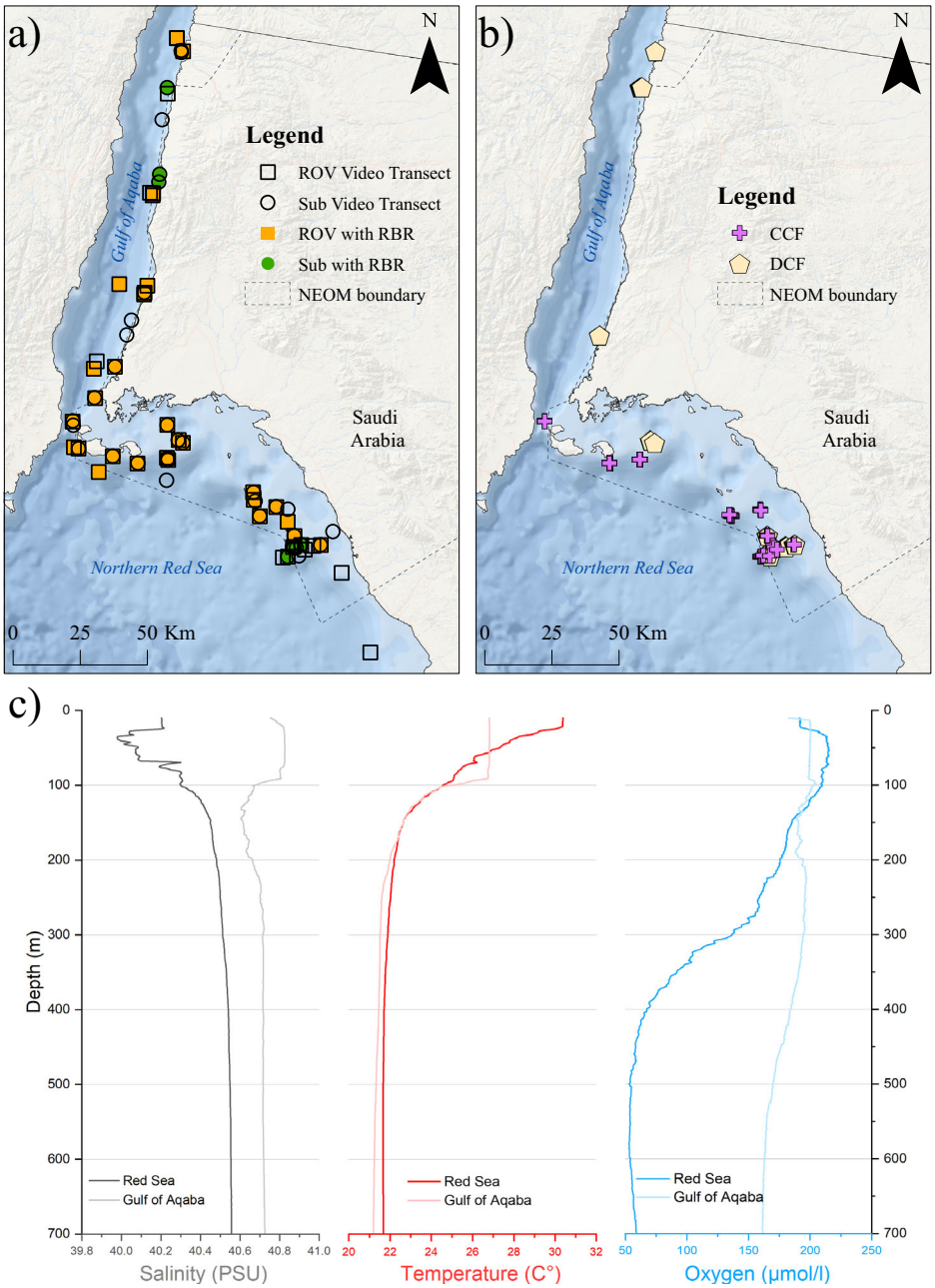

Fig. 1 | Distribution of data collection and framework observations in the northern Red Sea and Gulf of Aqaba. a Georeferenced video transects were recorded with submersibles (subs in open or green circles) and a Remotely Operated Vehicle (ROV in open of orange squares), mounted with a multiparametric probe (RBR, indicated by filled symbols) to measure environmental conditions. **b** Locations of Caryophylliidae Coral Framework (CCF, shown as crosses) and Dendrophylliidae Coral Framework (DCF, shown as pentagons) as identified from the videos. **c** Salinity (black), temperature (red) and dissolved oxygen concentration (blue) profiles varied between the Gulf of Aqaba (faded lines) and northern Red Sea (strong lines). NEOM refers to the giga-project in northern Saudi Arabia (neom.com) and is indicated in the maps by a dashed line. Basemap sources: ESRI, GEBCO, NOAA, National Geographic, Garmin, HERE, Geonames.org.

Following the stepwise selection process to retain only the most appropriate predictor variables, the final model for CCF was generated with eight variables (listed in order of their contribution to the model); Vector Ruggedness Measure (VRM-3), Local Convexity Index (CX-11), dissolved oxygen concentration, Terrain Surface Texture (TEX-3), depth, backscatter, Bathymetric Position Index (BPI-65) and aspect (Northness) (Tables 1 and 3). From a total of 206 presence points, 145 (approximately 70%) were used for the training dataset, while 61 were retained for testing. Model performance was high; the accuracy was 85.7%, the mean test AUC was 0.9867 and the mean training AUC was 0.9874. A small difference of only 0.0007 between test and training AUC values suggests that our model did not suffer from overfitting[76].

The highest percent contribution to the model was given by VRM-3 (52.2%), followed by CX-11 (23.9%; Table 3). Areas of High Habitat Suitability (AHHS) above the threshold of 0.75, were found at the lower end of the ranges of both VRM-3 and CX-11 (Fig. S2a; Table S3). They also occurred in areas with a narrow temperature range. The results of the jackknifing analysis show that the AUC remained extremely high when any individual variable was removed from the model, suggesting that there is redundancy in the information captured in each variable. On the other hand, VRM-3 contains the most useful information by itself, evident from the high test AUC for a model built with only VRM-3.

Overall, 102.5 km^2 of seafloor in the study area was predicted to have a habitat suitability over 0.75 (Table 3), covering 5.5% of the seafloor area between 300 and 700 m, the depth range in which the framework was identified (Table S3). The majority of AHHS were identified from the Northern Red Sea, with only one small area (200 m2) identified at the entrance to the Gulf of Aqaba (Straits of Tiran). An area of 217.9 km^2 had a habitat suitability between 0.5 and 0.75 (Table 3; Fig. 5a–c). AHHS were widespread in the Northern Red Sea, with many relatively large areas (e.g. over 20 km^2) identified to have low to medium suitability, and a few key areas with higher suitability, such as around Tiran and Sanafir Islands, and close to Duba port (Fig. 5c). Standard deviation (SD) of the habitat suitability was below 0.28, with an average value of 0.00014. Just 2.7 km^2 (0.01% of the total study area) had a SD between 0.2 and 0.28, while 256 km^2 (0.58% of the study area) had a SD in the range 0.1–0.2 (Fig. S3a).

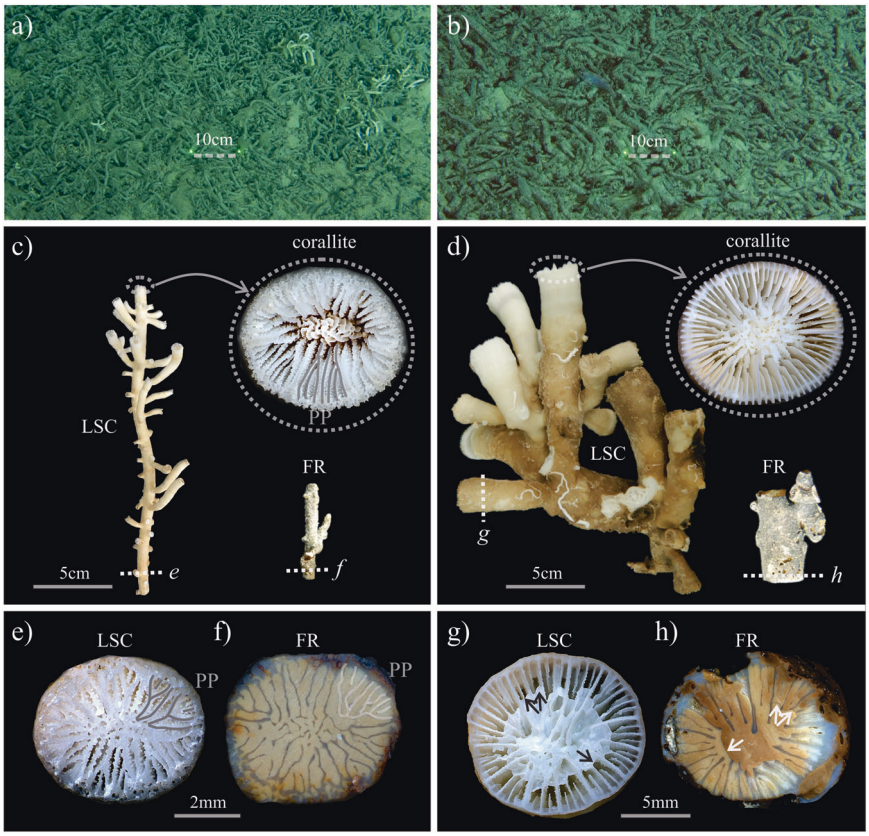

Fig. 2 | Identification process for the coral and coral framework specimens. Identification was conducted from **a**, **b** field images to **c**–**g** specimen diagnostic features examination. Examples are the Dendrophylliidae *Eguchipsammia fistula* (**a**, **c**, **e**, **f**), and the Caryophylliidae *Rhizosmilia valida* (**b**, **d**, **g**, **h**). Diagnostic features observed in the coralla of coral specimens collected alive (Live Specimen Corallum = LSC) and coral rubble detached from a solid framework (Framework Rubble = FR) include branch thickness, and columella and septal structure and arrangement visible in (LSC) corallites from collected coralla (**c**, **d**), and in fresh and fossil (FR) material transverse sections (**e**–**h**). In the Dendrophylliidae, the autapomorphic and diagnostic pattern of septal fusion called Pourtales Plan (PP, highlighted by overlying transparent lines) can be recognised in **c** the corallites and in the **e** LSC and **f** FR sections. In the Caryophylliidae branch sections, the typical columellar structure (arrows) can be recognised both in **g** fresh and **h** fossil material. Branch thickness is consistently thinner (< 2 cm) in the Dendrophylliidae and thicker (> 2 cm) in the Caryophylliidae, which also allows identification in the field when the laser pointers are used for scale (green dots 10 cm apart in **a** and **b**).

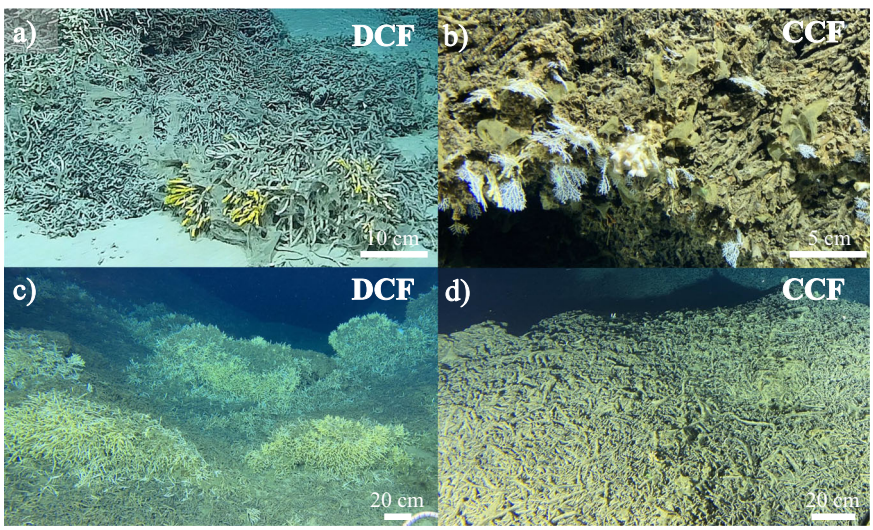

Fig. 3 | Two types of coral frameworks were identified. Two identified frameworks, **a** and **c** Dendrophylliidae Coral Framework (DCF), and **b** and **d** Caryophylliidae Coral Framework (CCF). In **b**, the white fan-shaped colonies belong to the hydrocoral *Stylaster tritoni* Maggioni, Cairns, Pica & Benzoni, 2022 growing on the CCF. All images were captured during the Deep Blue Expedition 2020 or the Red Sea Relationship Cultivation mission 2022 at depths **a** 376 m, **b** 420 m, **c** 416 m and **d** 429 m.

Dendrophylliidae Coral Framework (DCF)

Dendrophylliidae coral framework (DCF) was identified in 10 dives throughout the study region. It was found to be overlapping in range with CCF in the South, as well as extending to the northern Gulf of Aqaba, close to the Jordanian border. Additional locations were also identified close to Shushah Island, and in three locations in the Gulf of Aqaba (Fig. 5d–f).

For the final model for DCF habitat suitability, 11 predictor variables were included in the best-performing model (in order of contribution to the model); depth, VRM-11, TEX-5, CX-11, CI-11, seafloor rugosity, temperature, dissolved oxygen concentration, BPI-33, aspect (East) and salinity (Tables 1 and 3). A total of 124 presence points were used; 87 to train the model, and 37 as test data. The resulting model performed well, with an accuracy of 82.6%, a training AUC of 0.9902 and a test AUC of 0.9893. Again, the small difference between these two AUC values (0.0009) indicates an appropriate model fit, without overfitting[76].

The most informative variables to determine AHHS for DCF were depth, with a contribution of 35.8%, and VRM-11, which contributed 32.2% (Table 4). Both depth and VRM-11 had relatively restricted ranges in areas highly suitable for DCF (Fig S2b; Table S3), while aspect (East) and oxygen concentration demonstrated larger ranges within AHHS. From the jackknifing analysis, it is clear that depth contained the most unique information, as it results in the lowest test AUC for any individual variable removed, as well as providing the best model for a single variable.

https://doi.org/10.1038/s43247-024-01830-9

Table 1 | An explanation of the data used in the final models, including a biological justification for their use

	Parameter	Source	Software used	Window size (s)	Description of parameter	Biological relevance
	Water depth	Bathymetry	QPS Qimera	-	The depth of the water derived from the bathymetry	Many species are adapted to specific depth ranges[138]
	Backscatter	Kongsberg multibeam	QPS FGMT	-	A measure of seafloor hardness based on acoustic backscatter	Coral larvae require a hard substrate for settlement, sedimentation reduces settlement[139]
	Slope	Bathymetry	ArcMap	-	The degree of steepness of the seafloor, from flat areas to vertical walls	Influences current flow and food availability; different communities are found on walls to flat areas[140]
	Aspect (Eastness)	Bathymetry	ArcMap	-	The direction of the slope from −1 to 1, East to West; sin(aspect)	Influences local and regional currents and food availability[140]
	Aspect (Northness)	Bathymetry	ArcMap	-	The direction of the slope from −1 to 1, North to South; cos(aspect)	Influences local and regional currents and food availability[140]
Seafloor complexity	Bathymetric Position Index (BPI)	Bathymetry	ArcMap	3, 5, 9, 17, 25, 33, 65	Whether a point is elevated (crest), depressed (trough) or flat in comparison to the surrounding environment	Complexity of the seafloor can influence currents, food availability, and settlement[140]
	Vector Ruggedness Measure (VRM)	Bathymetry	ArcMap	3, 5, 11	A measure that combines the slope and rugosity, where low values can be either flat or steep, but higher values represent steep, rugose areas	May indicate presence of niches and areas of increased current[109]
	Terrain surface texture (TEX)	Bathymetry	Saga	3, 5, 11	Local variation in seafloor complexity, including frequency of positive and negative relief structures	May indicate habitat changes and is related to colonisation[113,140]
Curvature	Mean Curvature	Bathymetry	ArcMap	-	The average curvature of the seafloor across an area	Can be used to describe bathymetric features which may be preferred habitat[140]
	Profile curvature	Bathymetry	ArcMap	-	The curvature along the profile of the steepest slope	Can be used to identify the convexity or concavity of slopes[140]
	Planar curvature	Bathymetry	ArcMap	-	The curvature perpendicular to the slope, describing rate of change of the slope	Related to the convergence or divergence of current flow, and therefore food availability[140]
	Local convexity index (CX)	Bathymetry	Saga	3, 5, 11	Identifies the frequency of positive relief structures (convexity) in an area surrounding a central point	May indicate presence of features such as mounds[113]
	Convergence index (CI)	Bathymetry	Saga	3, 5, 11	Measures whether the slope converges to or diverges from a central point	May be used to identify features such as ridges or pits[121]
Environmental	Dissolved oxygen concentration	RBR sensor	ODV, ArcMap	-	The dissolved oxygen concentration in µmol/l at the seafloor	Can be used as a measure of carbon saturation state, important for coral growth and survival[141]
	Salinity	RBR sensor	ODV, ArcMap	-	The salinity in PSU at the seafloor	Can influence coral growth and survival[142]
	Temperature	RBR sensor	ODV, ArcMap	-	The temperature in °C at the seafloor	Corals may have specific temperature requirements that could correspond to depth; important for growth and survival[142,143]

Window sizes are shown in pixels. All parameters were processed to 30 m.

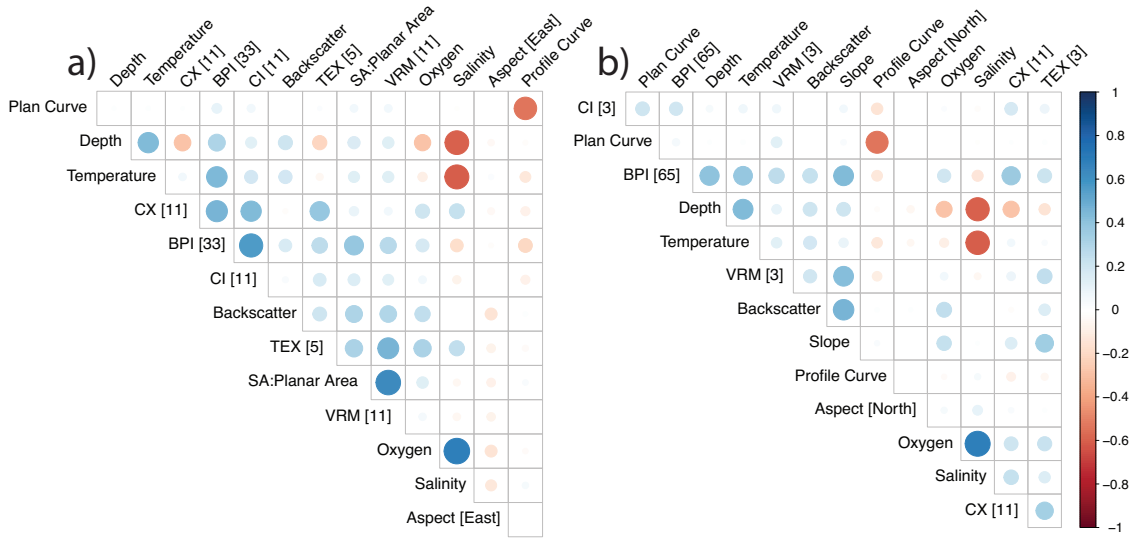

Fig. 4 | A correlation matrix between variables used in models. Variable correlations are shown for **a** Dendrophylliidae Coral Framework (DCF) and **b** Caryophylliidae Coral Framework (CCF). Larger circles and more intense colour indicates higher correlation, positive correlations are shown in blue, and negative correlations in red. Numbers after the variable name indicate the resolution of the variable. Acronyms used are VRM vector ruggedness measure, BPI bathymetric positioning index, CI convergence index, CX local convexity index and TEX terrain surface texture.

Table 2 | User's and producer's accuracy for model validation, based on spatially independent data collection for the two models, representing CCF (Caryophylliidae Coral Framework DCF (Dendrophylliidae Coral Framework)

		Ground truth		
		CCF	Not CCF	**User's accuracy**
Modelled	CCF	1	2	**33.3%**
	Not CCF	1	17	**94.4%**
	Producer's accuracy	**50.0%**	**89.5%**	

Overall accuracy: 85.7%

		Ground truth		
		DCF	Not DCF	**User's accuracy**
Modelled	DCF	1	4	**20.0%**
	Not DCF	0	18	**100.0%**
	Producer's accuracy	**100.0%**	**81.8%**	

Overall accuracy: 82.6%

Modelled (predicted) results are shown in the rows, while actual ground-truth data is shown in the columns. Values along the diagonal indicate correctly predicted framework presence or absence, while values above the diagonal represent errors of commission, and values below the diagonal represent errors of omission.

Across the northern Red Sea and Gulf of Aqaba, 155.2 km^2 of seabed was predicted to be highly suitable (> 0.75; Table 4; Fig. 5d–f). This represents 16.0% of the area within a suitable depth range (150–500 m). Approximately 87% (104.9 km^2) of this area occurs in the northern Red Sea. There are three main areas in which AHHS is concentrated. The most northerly is found in the Gulf of Aqaba, beginning close to the Jordanian border, and extending south along the coast, intermittently over about 50 km, including the area in front of the small city of Haql (Fig. 5e). The second area is identified to the East of Sanafir Island in the northern Red Sea, within the NEOM Bay (Fig. 5f). This area includes approximately 7.9 km^2 of highly suitable habitat close to the coast of Shushah Island. SD of the habitat suitability was comparable to that of CCF, remaining below 0.28, with an average value of 0.00019. Here, 16 km^2 (0.04% of the study area) had a SD in the range 0.2–0.28, while 309 km^2 (0.70% of the study area) had a SD between 0.1 and 0.2 (Fig. S3b).

Discussion

The results presented here considerably expand the current state of knowledge on the benthic environment of the deep Red Sea. Deep sea corals have previously been identified from the Red Sea[40,43–46,77,78], but their spatial distribution remains understudied. Based on observations made during 20 dives conducted with an ROV and subs, as well as environmental and geomorphometric variables, we have generated the first large-scale, high-resolution (30 m resolution) habitat suitability model for two types of deep coral frameworks in the Red Sea. We have found that both Caryophylliidae and Dendrophylliidae frameworks are each likely to occupy over 100 km^2 of seafloor in the northern Red Sea, and DCF is also likely to cover almost 50 km^2 in the Gulf of Aqaba. These values represent a high percentage of the depth range where the frameworks were observed (5.5% of 300–700 m for CCF and 16.0% of 150–500 m for DCF). The reliability of these results, due to high performance metrics (AUC value), and the relative ease of modelling habitat forming species[79], increases their value in conservation planning[80]. When compared to data from the Allen Coral Atlas[81], we found these deep coral frameworks to be equivalent to at least 35% of the area of shallow reefs in the same region.

These Red Sea coral frameworks are formed by species of the families Dendrophylliidae and Caryophylliidae, families which are also known framework builders in cold-water environments, usually associated with deep, offshore areas[82]. Caryophylliidae (e.g., *Goniocorella Dumosa* (Alcock, 1902), *Desmophyllum pertusum* (Linnaeus, 1758) and

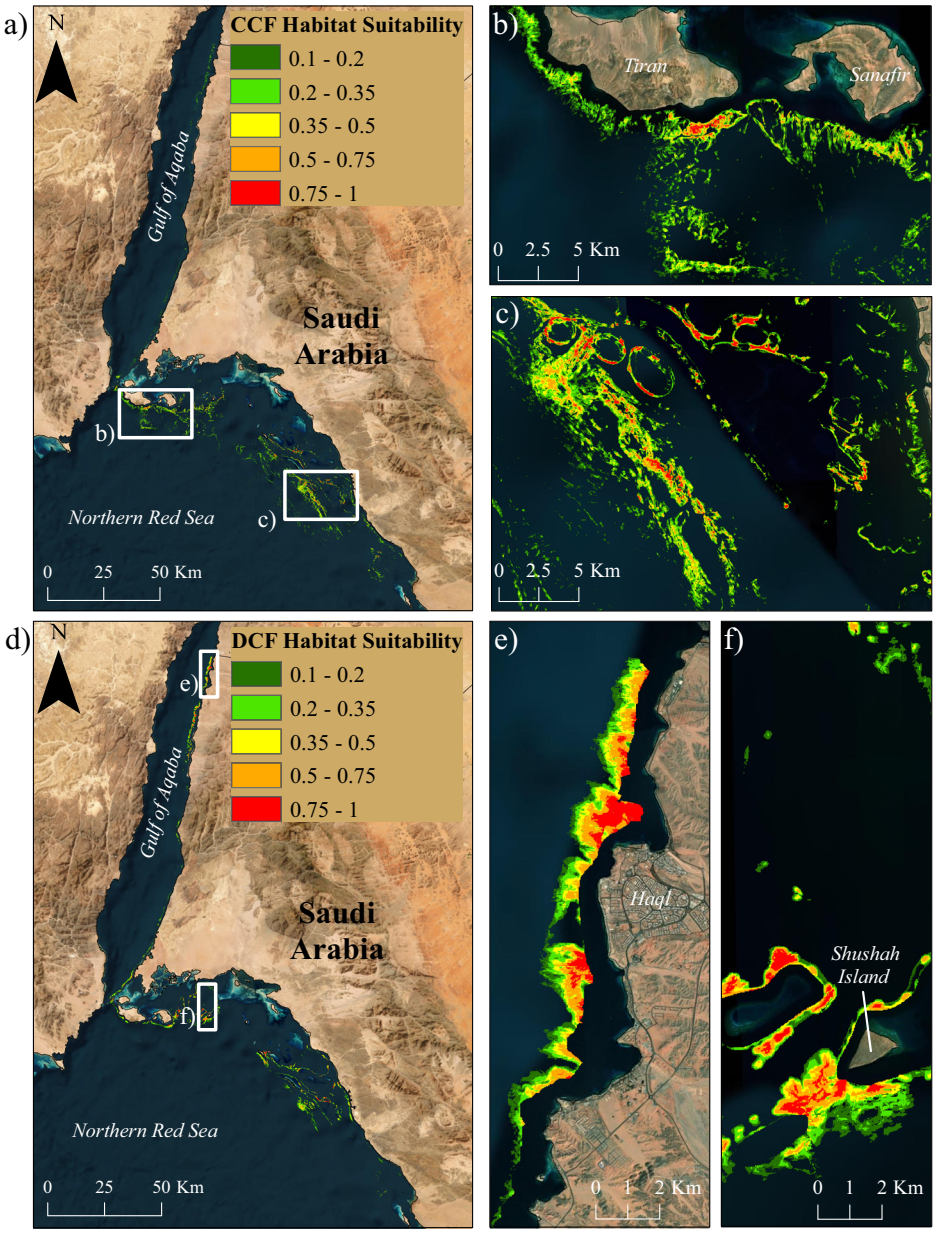

Fig. 5 | Results of habitat suitability models. Habitat suitability is shown for **a**–**c** Caryophylliidae Coral Framework (CCF) and **d**–**f** Dendrophylliidae Coral Framework (DCF). The highest habitat suitability is indicated in red, and values between 0-0.1 have been masked for visualisation. Satellite imagery source: ESRI, Maxar and Earthstar Geographics.

Solenosmilia variabilis Duncan, 1873) and Dendrophylliidae (e.g., *Enallopsammia rostrata* (Pourtalès, 1878)) are well represented among common framework-building species in deep cold-water environments[83]. Although different representatives of these families occur commonly throughout the Red Sea, they do not always form frameworks. For example, *E. fistula* does not always form DCF, as it was also identified as an associated species of CCF (e.g., sub-dive NTN0048). The formation of frameworks is not always inevitable, and some species may require an environmental or geological trigger, such as hard substrates[84,85] or strong currents[86]. The coral carpets of Oman and Yemen provide an example from a shallower ecosystem[87]. These species occur despite being unable to build frameworks or reefs[87]. Once a three-dimensional structure is present, however, sediment is trapped by the structure and current patterns are altered, creating a positive feedback mechanism and encouraging the growth of the framework[16,88]. *Desmophyllum pertusum* is widespread in cold-water environments, but only forms reefs in areas with hard bedrock substrate and features such as mounds or banks[86]. Framework-building species are, therefore, distributed more widely than the frameworks themselves.

Fundamental differences between the northern Red Sea and the Gulf of Aqaba are reflected in the distribution of both CCF and DCF. While CCF is absent from the Gulf of Aqaba aside from a small 1 km^2 area in the South, DCF is present in the Northern Gulf of Aqaba (Fig. 5). DCF differs in the main framework-building species; it is built by *E. fistula* in the northern Red Sea and by *D.* cf *cornigera* in the Gulf of Aqaba. These differences are influenced by variations in environmental and geomorphometric conditions between the two water bodies. Temperatures are slightly higher in the northern Red Sea, while salinities are marginally higher in the Gulf of Aqaba (Fig. 1c). Furthermore, the central Gulf of Aqaba is characterised by steeper slopes than the rest of our study area[41,89], which may explain the absence of DCF in this area. There was also an observed difference in depth range in DCF, with an average depth of 445 m in the northern Red Sea and 265 m in the Gulf of Aqaba, likely due to the environmental tolerances of the two species. Depth was also the predictor with the highest explanatory power in the model for DCF (Table 4) and has been shown elsewhere to be extremely important in determining community composition[14,15,25,89]. Environmental gradients in temperature, salinity and oxygen concentration across the study area (Fig. 1c) are driven by the flow of warm water over the shallow Strait of

Table 3 | Total area identified by habitat suitability models for five bands of habitat suitability, for two assemblages, Caryophyllidae Coral Framework (CCF) and Dendrophylliidae Coral Framework (DCF)

CCF		DCF	
Probability	**Area km²**	**Probability**	**Area km²**
>0.75	102.51	>0.75	155.24
0.5–0.75	217.91	0.5–0.75	282.59
0.35–0.5	355.90	0.35–0.5	292.79
0.2–0.35	882.38	0.2–0.35	608.20
0.1–0.2	1557.73	0.1–0.2	883.31
0.1–1	3013.91	0.1–1	2066.88

Table 4 | Percent contribution of each variable to the final model for Caryophylliidae Coral Framework (CCF) and Dendrophylliidae Coral Framework (DCF)

CCF		DCF	
Variable	**% contribution**	**Variable**	**% contribution**
VRM-3	52.2	Depth	35.8
CX-11	23.9	VRM-11	32.2
Dissolved oxygen concentration	8.3	TEX-5	8.0
TEX-3	5.9	CX-11	6.7
Depth	5.0	CI-11	5.0
Backscatter	2.8	Rugosity	4.0
BPI-65	1.7	Temperature	2.8
Aspect [North]	0.1	Dissolved oxygen concentration	2.6
		BPI-33	2.3
		Aspect [East]	0.6
		Salinity	0.1

Tiran, and the lagoon-like circulation within the Gulf of Aqaba[90]. All three environmental variables that were included remained in the final model for DCF, while dissolved oxygen concentration was one of the most important variables for CCF, in agreement with previous work that has shown how environmental variables improve habitat suitability models[91]. CCF may be limited to the northern Red Sea due to these differences in dissolved oxygen concentration, suggesting that it could be close to the edge of its range in the Straits of Tiran. The interpolation of the environmental variables results in layers that, although presented at 30 m, are potentially less detailed, and may miss small-scale patterns. This could potentially result in an underestimation of their influence on the models compared to geomorphological data.

There is strong evidence that the distribution of these frameworks extends further outside the extent of our study area. A coral framework reported by Qurban et al.[44] is dominated by *E. fistula* and is identified here one of the main builders for DCF. This point, located at 640 m depth, was outside of the extent of this study, so we were not able to compare this presence to our model results, although reported temperature (21.47 °C) and salinity (40.54 PSU) values were comparable to ours (Fig. 1c). This report indicates that we have not explored the whole range for DCF; it likely occurs deeper and further south than our observations. Additionally, the area in the Northern Gulf of Aqaba suggests that these frameworks may also be present close to Eilat, however only coral rubble fields are known to be present in the mesophotic[89], and no deep coral frameworks have been reported, despite a concentration of mesophotic and deep studies in this region[17,92,93].

Large areas of our study region may be occupied by coral framework, indicating a previously unknown light-independent carbonate factory in the deep Red Sea. A recent review of carbonate systems by Reijmer[94] classifies five types, listing light and temperature as the main determining characteristics. Due to the uniquely warm aphotic zone of the Red Sea, this environment does not fit within the constraints provided for any of the described carbonate systems, highlighting how this environment has been so far overlooked in the literature. Both reef and non-reef environments in the shallow and mesophotic zones of the Red Sea are considered to be productive carbonate factories[95–98], but these systems differ in their trophic structure to deeper reefs, as organisms change from autotrophic to heterotrophic, and their influence on the carbon cycle changes accordingly[99]. Accretion rates of shallow-water reefs have been estimated to fall between 0.67 and 1.5 m/kyr[100,101]. The growth rate of *D. cornigera*, as well as three other cold-water corals was calculated on samples from the Mediterranean[102]. The results of this study found the growth rate of *D. cornigera* to be 0.04 % growth per day when samples were kept at 12 °C[102]. With further information on the potential difference of these growth rates in Red Sea conditions, up to 10 °C warmer, we may be able to calculate the timeframe of reef development or the carbon source potential of these coral frameworks[103,104]. Furthermore, variation in growth rates[105,106] and forms of founding species may influence the framework accretion rate. For example, the porous, brittle form of dendrophylliids[71,107,108] could result in increased breakage, which may lead to less vertical growth, but more propagation, increasing the horizontal area of the framework, in comparison to the denser and more compact form of caryophylliids[71,107].

One of the limitations of this study is the exclusion of a number of environmental and biological factors that may influence the distribution of these frameworks, such as water chemistries, species connectivity or competition. Due to the complexity of contributing factors to the distribution of a species or assemblage, as well as the difficulty of measuring some parameters, many of the predictor variables are used to act as a proxy for one or more other components of the environment that are difficult to measure or record, such as those mentioned above. For example, as in Bargain et al.[26], vector ruggedness measure (VRM)[109] contributed highly to our models. VRM is intended as a measure of seafloor complexity, however, it can act as a proxy for current velocity, as currents are strongly influenced by local geomorphology, especially as rugosity is scale independent[110]. In turn, current velocity can influence spatial patterns of larval distribution, as well as food availability to benthic organisms[16,88,111,112]. While VRM is not as accurate as true measures of current velocity, a combination of geomorphometric parameters can provide vital information. For example, terrain surface texture, another measure of complexity (focusing on the presence of pits and peaks in the bathymetry), was also selected for both models[113]. Furthermore, VRM may provide some information on the substrate type, as large areas of soft substrate, such as mobile sediment, will have a low complexity. Numerous habitat suitability models for deep-sea species and assemblages have been published[26,56,86,114,115], but this is the first example from the deep and warm Red Sea. Comparisons between models are difficult due to differences in field sampling, the ecology of the study species, and the methods used for MaxEnt modelling[116]. Additionally, the parameters used by MaxEnt are often not reported in papers, making it difficult to establish standardised methodology and discuss differences, or lack thereof, among localities and conditions[116].

This exploration of the deep Red Sea comes at an important time for Saudi Arabia, as the Kingdom is currently developing a number of large-scale 'Giga Projects', as part of their Vision 2030 plan (vision2030.gov.sa)[117]. The largest of these projects is NEOM, based in the northwest of the Kingdom (Fig. 1a; neom.com), where our study site is located. While Saudi Arabia has ambitious environmental goals for NEOM, it is inevitable that the surrounding environment will be somewhat impacted during the construction phase. Coastal development may increase the sediment load in the water column, which has been shown to cause mortality in deep water corals[118]. This may be a particular problem for deep reefs when the continental margin is very steep, such as the Gulf of Aqaba, where deep reefs are

found much closer to the shore. Additionally, an area over 7 km^2 that was highly suitable for DCF close to Shushah Island, which could become an important and biodiverse reserve for NEOM. A better understanding of the spatial distribution of highly biodiverse communities, such as deep coral frameworks, could improve conservation planning in areas important for these large projects.

Extreme caution is required when interpreting the results of habitat suitability models[69], as they are based on modelled data, and high local heterogeneity in species distribution can cause overestimates[119]. The most reliable models are rigorously validated using extensive independent datasets, while we have included some independent validation here, further data would improve this reliability. However, when used and assessed correctly, models can be incorporated into spatial planning practices to increase available data resolution, although this is still not common practise[80]. Here, we provide information that can inform management of deep-sea ecosystems in the NEOM region. It is also vital to consider that these assemblages contain both the framework-building species and ecologically important associated fauna, including cryptic organisms and meiofauna[18,23,51–53]. Focusing on the whole assemblage instead of a single species can be more useful for conservation as it ensures the protection of understudied and cryptic species[86,119].

We report the distribution of previously unknown potential habitats for deep coral frameworks in the northern Red Sea and Gulf of Aqaba, built by corals from the families Caryophylliidae and Dendrophylliidae. The extent of these frameworks is likely to be much larger than currently known, encompassing over 10% of our 33,970 km^2 study region between 150 and 700 m depth, based on the results of habitat suitability models. We have presented important discoveries here, but more research is necessary to fully understand these deep, warm-water coral frameworks. For example, further investigation should focus on quantifying the growth rates of these species, and the role of microbes in accretion of these frameworks[120] in order to better understand the potential of a deep, Red Sea carbonate factory. Dating of the coral rubble to understand the conditions during initial framework formation may provide further understanding of the mechanisms which trigger formation of such structures. Finally, these frameworks provide habitat, shelter and settlement opportunities for associated fauna, much of which remains understudied. It is clear that many questions remain about these frameworks, and they could become an important and informative study system for many fields. Our results on their abundance and distribution can provide essential information for conservation planning at a crucial time for the region.

Methods

Acoustic data

We focused on an area in the northern Red Sea and Saudi Arabian Gulf of Aqaba, mostly within the jurisdiction of NEOM (Fig. 1a). The Gulf of Aqaba is characterised by steep slopes, and is separated from the northern Red Sea by a shallow sill (Tiran Strait) that restricts water movement[41]. Bathymetry and backscatter data were acquired down to a depth of 1760 m over an area of 33,970 km^2 during the Deep Blue Expedition aboard the M/V OceanXplorer. This research cruise lasted six weeks between October and November 2020. A 30 kHz Kongsberg EM304 hull-mounted multi-beam echosounder was used alongside the acquisition software QPS Qinsy, before being post-processed to a resolution of 30 m with QPS Qimera (V. 2.4.1) and FMGT (V. 7.10.0) for bathymetry and backscatter respectively. Sound velocity profiles, used to calibrate the multi-beam acquisition, were collected with 29 eXpendable BathyThermographs (XBT).

Geomorphometric parameters[121] were extracted from the multi-beam bathymetry surface using ArcMap v10.8 and Saga v8.1.1[122] using default settings other than the window sizes (as in Table 1), according to Bargain et al.[26]. The geomorphometric parameters were selected to represent different characteristics of the seafloor morphology, using window sizes that represent both extremely local and broader scales (Table 1). A combination of these parameters can act as a proxy for other environmental variables, such as current velocity, which play a strong role in the location of coral assemblages (for further detail, see ref. 123).

Environmental data

Temperature, salinity and dissolved oxygen concentration were collected using an RBR *maestro3* logger, using sensors (Marine CT for temperature, Marine CT 2000m for conductivity RBRcoda T.ODO|fast for dissolved oxygen concentration) mounted onto either the Remotely Operated Vehicle (ROV) or a submersible (sub; Fig. 1a). These sensors allowed continuous recording of near-bottom conditions along each transect. We separated these data into ten depth ranges based on three distinct layers of water identified in both the northern Red Sea and the Gulf of Aqaba. The upper layer, extending from the sea surface to the base of the thermocline, approximately 300 m deep, experiences notable temperature fluctuations driven by solar radiation and seasonal changes, with the thermocline marking the temperature changes sharply with depth. Below lies the middle layer, spanning from 300 to 600 m, characterised by low oxygen levels, creating an oxygen minimum layer due to reduced mixing and biological processes. Lastly, the deep layer extends from 600 m to the seafloor, where temperature and oxygen concentrations remain relatively constant. These three layers were further partitioned to account for smaller scale environmental patterns along the depth gradient, which are most likely in the upper layer (Fig. 1c). For the upper layer, six layers of 50 m were used (0–50 m, 50–100 m, 100–150 m, 150–200 m, 200–250 m and 250–300 m); for the middle of the water column, data was separated into layers of 100 m (300–400 m, 400–500 m and 500–600 m), and finally, all data below 600 m was combined into a single layer (600–1700 m). We ensured that for each depth layer there were sufficient (> 200) measurements in both the northern Red Sea and in the Gulf of Aqaba. The surface layer (0–50 m) had 44 data points from seven dives, but as it is much shallower than the observed range of our assemblages of interest, this is unlikely to impact our results. For each of the other layers, the number of data points was between 297 and 1744, from 8–21 dives. In Ocean Data View (ODV[124]), each layer was loaded separately, and data was interpolated using the Data-Interpolation Variational Analysis (DIVA) function. The resulting rasters were imported to ArcMap v10.8 and interpolated with Inverse Distance Weighted (IDW) using default settings in ArcMap v10.8 to create a continuous raster across the study region for each variable at each depth range (30 rasters total). We selected IDW to improve separation between the northern Red Sea and Gulf of Aqaba. However, IDW relies on regular data points and may overlook small-scale patterns if the data coverage is insufficient. Furthermore, it places the same weight on all neighbouring data points, which can result in greater influence of potential outliers[125]. We were careful here to assess our dataset for erroneous data before proceeding. Finally, rasters were clipped to the depth layer they represent, and merged, creating a final 30 m resolution layer file for each variable. While this step would often utilise remotely sensed satellite data (e.g., BioOracle[126]), we examined the data available for the seafloor in the Northern Red Sea, and found highly anomalous variables. Furthermore, the resolution of remotely sensed data is 5 arcmin (approximately 9.2 km for our study area), much coarser than the interpolated datasets that we created. Additional environmental parameters, such as pH or aragonite saturation state, may be informative to this study, but were not directly measured here and can therefore not be interpolated.

Sampling, identification and video analysis

During the same Deep Blue Expedition, video transects were recorded using two Triton 3300/3 submersibles (subs) and a work-class ARGUS Mariner 108 XL ROV. Videos were obtained with Arctic Rays EagleRay 4 K cameras with 4 K Atmos Shogun monitors from both the ROV (Chimaera, CHR) and one of the subs (Neptune, NTN). The ROV also had an HDTV 1080p F/Z Colour camera. A Wide-Angle Red DSMC2 Helium 8 K Canon CN-E15.5-47 mm lens and a macro Red DSMC2 Helium 8 K Nikon ED 70–180 mm F4.5-5.6D were used on board the second sub (Nadir, NDR). Due to limited previous sampling in the region, the nature of this expedition was exploratory, and sites were selected with the aim of covering a diverse range of seafloor morphologies, and their associated ecosystems. A total of 49 sites were surveyed (21 from the ROV and 28 from the sub), generating over 300 h of high-resolution video. The video transects were georeferenced

using the positioning system of each vehicle: (a) a Kongsberg HIPaP 501 USBL (Ultra-Short Baseline) and Sonardyne Sprin INS (Inertial Navigation System) on the ROV and (b) a Sonardyne Ranger Pro 2 USBL on each sub. Finally, Shilling T4 hydraulic manipulators were mounted on the ROV and Neptune sub for specimen collection.

For each of these dives, video of the benthic habitat was recorded and later classified into broad assemblages using ArcGIS. The transect lines were mapped and matched to the video via the time stamp. Each coordinate point was then classified based on the dominant taxa (i.e., the taxa that forms the structure), as well as associated benthic fauna and the substrate. From the resulting analysis, two unique assemblages with potentially high conservation values were identified for predictive modeling. These assemblages are named 'Dendrophylliidae Coral Framework' (DCF; Figs. 1b and 3) and 'Caryophylliidae Coral Framework' (CCF; Figs. 1d and Fig. 3). These frameworks were identified from the videos due to the 3D structure which changes the shape of the seafloor, and the large areas of rubble which usually surrounds the live colonies, resulting from the breakdown of the structure. The live area of the framework was identified to family and, where possible, species level (Fig. 2). When only the dead rubble was present, the framework was still classified according to the family, based on its morphology and corallite diameter size class (see hereafter).

Identification of coral taxa and rubble in the videos was performed based on a collection of living and rubble specimens with the manipulator arm of the ROV or sub. After tagging, live specimens were subsampled to preserve soft tissue in 99% ethanol for further molecular analysis. The rest of the specimen was cleaned with a solution of sodium hypochlorite overnight, rinsed in freshwater and dried for observation of diagnostic features. We measured the branch diameter of dead rubble and freshly collected specimens with a caliper. Septal arrangement pattern was examined in the corallites of the specimens collected alive and in the transversal section to the corallite growth axis in both alive and rubble-collected material. Imaging was performed using a Leica M205A stereomicroscope with a Leica DMC 5004 camera. The presence of the diagnostic septal fusion pattern called Pourtalès Plan (PP) allowed the identification of Dendrophylliidae taxa. All rubble and living collected specimens with PP had corallite diameter smaller than 1 cm. Caryophylliidae specimens, all lacking PP, had corallite diameter larger than 1 cm, thus allowing ground-truthing in the identification from the videos. References from the literature were used for identifying Dendrophylliidae (*Eguchipsammia fistula* and *Dendrophyllia* cf *cornigera*[71,107,108]) and Caryophylliidae (*Rhizosmilia valida* and *Caryophyllia* sp.[71,127]).

Model development

Models were developed separately for the two assemblages, CCF and DCF. All environmental and geomorphometric data was clipped to the same extent in R (R Studio v4.1.2[128]), based on the backscatter, which had the smallest extent and prepared as ASCII raster files. Correlations between all variables were assessed through a Pearson's correlation analysis in R. We based our methodology on previously published studies with similar sampling regimes[26,63,86,129]. A maximum entropy algorithm was used to model the data, using MaxEnt (V. 3.4.4[65,130]) to run the models. MaxEnt was selected as the sole algorithm to run the models as it requires presence-only input data, and has regularly been shown to produce the best and most reliable models among different species and habtiats[67–70,131]. While ensemble models have sometimes been shown to improve model results[62], other studies report no benefit[132]. We opted not to run ensemble models as other algorithms have been shown to perform poorly with presence-only data, and may have negatively impacted our results. With more comprehensive sampling, abundance data could be used in place of presences, and absence data could be used in place of background points, both of which would improve accuracy[133]. However, this level of sampling is difficult in remote areas, as narrow transects do not allow confidence in absences[134]. Trials were conducted on an initial subset of the data to determine the best settings for MaxEnt; we used the AUC (Area Under the receiver operator characteristics Curve; as explained below) value for both training and test data to estimate whether different settings had a positive, negative or neutral effect on the model performance. From this, we decided to use only hinge features, with a regularisation multiplier of 2.5, to build a smoother model, and avoid overfitting to the training data[60,76,135]. Most other settings were kept at default (extrapolation and clamping enabled, convergence threshold = 0.00001, 10000 background points, 500 maximum iterations, and prevalence = 0.5), but some changes were made: ten replicates were carried out via a bootstrapping method, where each model was trained on 70% of the data and tested on the remaining 30% of the data. Duplicated presence points were removed through MaxEnt, resulting in spatially thinned data.

The AUC was used both to develop the model and later to validate the models (see below: Model Validation). It is calculated for both training data and test data, and gives an indication of the proportion of true positives and false positives, where a value closer to one indicates a better model performance. To select the best subset of predictor variables, a stepwise selection process was used, following the workflow of Kinlan et al.[115]. An initial model was run, using all potential variables, with jack-knifing enabled to assess the importance of each variable to the model. The jack-knifing analysis repeats the model, systematically leaving out each predictor variable, resulting in an improved understanding of the contribution of each variable. The least useful variables, according to the jack-knifing analysis, were removed, and the process was repeated. At each stage, the test AUC value was recorded, and we continued the process until either there was only a single variable remaining or the test AUC had dropped to <95% of the initial value. The trial with the highest AUC determined the set of predictor variables that were used in the final model. This process avoids the overestimation of small trends in the data. Finally, among strongly correlated variables ($r^2 > 0.7$; Fig. 4), the variable with the highest overall contribution to the final model was retained, and the rest were not included in the model to reduce the chance of spatial autocorrelation among variables, therefore all final variables used were uncorrelated ($r^2 < 0.7$) according to a Pearson's correlation analysis (Fig. 4).

Model validation

Two statistics were used to assess the models, the Area Under the receiver operator characteristics Curve (AUC), and the True Skills Statistic (TSS). TSS is calculated based on errors of omission and commission, on a scale from −1, indicating complete disagreement, to +1, signifying perfect agreement[136]. Here, we used the MaxSSS (Maximising the Sum of Sensitivity and Specificity) as the threshold in this calculation[137]. Additionally, the AUC metric is effective to compare between models based on the same data[66], and, therefore, provided effective evaluation during the iterative process to reduce predictor variables. However, the metric is less informative for standalone model evaluation based on presence-only data and may be extremely sensitive to autocorrelation. Despite the spatial thinning that was applied, we ran further tests to assess the influence of the autocorrelation on our models. Eleven clusters were identified among the presence points of both CCF and DCF (Fig. S4). Points were considered to be in the same cluster as any points within a 1000 m radius, resulting in some long clusters which extended over 1000 m in length. The final models were rerun 11 times, each time keeping one entire cluster of points as independent validation data. This allowed us to calculate the AUC value on data that is spatially independent. The size of each cluster varied, resulting in test datasets of between 1 and 24% (2 and 47 presence points out of a total of 206 for CCF, and between 2 and 29 points out of 124 for DCF).

While this was a thorough method to assess our models, the most reliable validation comes from ground-truth data. Unfortunately, this is also the most time consuming and costly method, and is not always possible. Fortuitously, in 2022, the M/V OceanXplorer collected data from ROV and sub-dives conducted in nearby areas in the northern Red Sea and Gulf of Aqaba during the Red Sea Relationship Cultivation mission. This data provided opportunistic ground-truth points for our models, which remain completely independent from our training data, and allow us to calculate the errors of omission and commission. Furthermore, published records from Qurban et al.[44] provide an additional independent validation point. While this ground-truth data is not extensive, it is extremely valuable in providing support to our methodological process and our results.

Reporting summary

Further information on research design is available in the Nature Portfolio Reporting Summary linked to this article.

Data availability

Data used in this study is available in this paper, Methods and Supplementary Materials. Additionally, relevant data that was used to generate these models, as well as results files, are available at https://doi.org/10.5281/zenodo.13935238.

Received: 17 April 2024; Accepted: 23 October 2024;
Published online: 16 November 2024

References

1. Hoegh-Guldberg, O. Coral reef ecosystems and anthropogenic climate change. *Region. Environ. Change* **11**, 215–227 (2011).
2. Margules, C. R. & Pressey, R. L. Systematic conservation planning. *Nature* **405**, 243–253 (2000).
3. Flower, J. et al. Marine spatial planning on the Caribbean island of Montserrat: lessons for data-limited small islands. *Conserv. Sci. Pract.* **2**, e158 (2020).
4. Knowlton, N. et al. *Life in the World's Oceans: Diversity, Distribution, and Abundance* Vol. 1 (ed. Alasdair D. M.) 65–77 (Wiley-Blackwell, 2010).
5. Moberg, F. & Folke, C. Ecological goods and services of coral reef ecosystems. *Ecol. Econ.* **29**, 215–233 (1999).
6. Woodhead, A. J., Hicks, C. C., Norström, A. V., Williams, G. J. & Graham, N. A. J. Coral reef ecosystem services in the Anthropocene. *Funct. Ecol.* **33**, 1023–1034 (2019).
7. Bakker, A. C. et al. Heat, human, hydrodynamic, and habitat drivers measured from space correlate with metrics of reef health across the South Pacific. *Coral Reefs* **42**, 219–238 (2023).
8. Benfield, S. L., Guzman, H. M., Mair, J. M., Young, J. A. T. & Guzman, H. M. Mapping the distribution of coral reefs and associated sublittoral habitats in Pacific Panama: a comparison of optical satellite sensors and classification methodologies. *Int. J. Remote Sens.* **28**, 5047–5070 (2007).
9. Hamylton, S. M. Mapping coral reef environments: a review of historical methods, recent advances and future opportunities. *Prog. Phys. Geogr.* **41**, 803–833 (2017).
10. Roelfsema, C., Phinn, S., Jupiter, S., Comley, J. & Albert, S. Mapping coral reefs at reef to reef-system scales, 10s–1000s km^2, using object-based image analysis. *Int. J. Remote Sens.* **34**, 6367–6388 (2013).
11. Saul, S. & Purkis, S. Semi-automated object-based classification of coral reef habitat using discrete choice models. *Remote Sens.* **7**, 15894–15916 (2015).
12. Purkis, S. J. et al. High-resolution habitat and bathymetry maps for 65,000 sq. km of Earth's remotest coral reefs. *Coral Reefs* **38**, 467–488 (2019).
13. Purkis, S. & Chirayath, V. Annual review of environment and resources remote sensing the ocean biosphere. *Annu. Rev. Environ. Resour.* **47**, 823–847 (2022).
14. Kahng, S. E. et al. Community ecology of mesophotic coral reef ecosystems. *Coral Reefs* **29**, 255–275 (2010).
15. Correa, T. B. S. et al. Variability of cold-water coral mounds in a high sediment input and tidal current regime, Straits of Florida. *Sedimentology* **59**, 1278–1304 (2012).
16. van der Kaaden, A. S. et al. Tiger reefs: Self-organized regular patterns in deep-sea cold-water coral reefs. *Ecosphere* **14**. https://doi.org/10.1002/ecs2.4654 (2023).
17. Eyal, G., Tamir, R., Kramer, N., Eyal-Shaham, L. & Loya, Y. The Red Sea: Israel. *Coral Reefs World* **12**, 199–214 (2019).
18. Bongiorni, L. et al. Deep-water scleractinian corals promote higher biodiversity in deep-sea meiofaunal assemblages along continental margins. *Biol. Conserv.* **143**, 1687–1700 (2010).
19. Nunes Peinemann, V. et al. First record of Boulenger's anthias Sacura Boulengeri (Heemstra 1973) in the Red Sea. *J. Fish Biol*. https://doi.org/10.1111/jfb.15254. (2022)
20. Cordes, E. E. et al. Expanding our view of the cold-water coral niche and accounting of the ecosystem services of the reef habitat. *Sci. Rep.* **13**. https://doi.org/10.1038/s41598-023-45559-5. (2023)
21. Armstrong, R. A., Pizarro, O. & Roman, C. Underwater robotic technology for imaging mesophotic coral ecosystems. *Coral Reefs World* **12**, 973–988 (2019).
22. Baker, K. D. et al. Distributional patterns of deep-sea coral assemblages in three submarine canyons off Newfoundland, Canada. *Mar. Ecol. Prog. Ser.* **445**, 235–249 (2012).
23. Robert, K., Jones, D. O. B., Georgiopoulou, A. & Huvenne, V. A. I. Cold-water coral assemblages on vertical walls from the Northeast Atlantic. *Divers. Distrib.* **26**, 284–298 (2019).
24. Ramos, A., Sanz, J. L., Ramil, F., Agudo, L. M. & Presas-Navarro, C. *Deep-Sea Ecosystems Off Mauritania: Research of Marine Biodiversity and Habitats in the Northwest African Margin.* 481–525 (Springer Netherlands, 2017).
25. Tamborrino, L. et al. Spatial distribution and morphometry of the Namibian coral mounds controlled by the hydrodynamic regime and outer-shelf topography. *Front. Mar. Sci.* **9** https://doi.org/10.3389/fmars.2022.877616 (2022)
26. Bargain, A., Marchese, F., Savini, A., Taviani, M. & Fabri, M.-C. Santa Maria di Leuca Province (Mediterranean Sea): identification of suitable mounds for cold-water coral settlement using geomorphometric proxies and Maxent methods. *Front. Mar. Sci.* **4**, 338 (2017).
27. Danovaro, R. et al. Towards a marine strategy for the deep Mediterranean sea: analysis of current ecological status. *Mar. Policy* **112**, 103781 (2020).
28. Lo Iacono, C., Savini, A., Huvenne, V. A. I. & Gràcia, E. *Mediterranean Cold-Water Corals: Past, Present and Future.* 157–171 (Springer, 2019).
29. Chimienti, G., Bo, M., Taviani, M. & Mastrototaro, F. *Mediterranean Cold-Water Corals: Past, Present and Future.* 213–243 (Springer, 2019).
30. Roberts, J. M. & Cairns, S. D. Cold-water corals in a changing ocean. *Curr. Opin. Environ. Sustain.* **7**, 118–126 (2014).
31. García-Ibáñez, M. I., Bates, N. R., Bakker, D. C. E., Fontela, M. & Velo, A. Cold-water corals in the Subpolar North Atlantic Ocean exposed to aragonite undersaturation if the 2 °C global warming target is not met. *Glob. Planet. Change* **201**. https://doi.org/10.1016/j.gloplacha.2021.103480 (2021).
32. Hennige, S. J. et al. Hidden impacts of ocean acidification to live and dead coral framework. *Proc. R. Soc. B Biol. Sci.* **282**. https://doi.org/10.1098/rspb.2015.0990 (2015).
33. Hennige, S. J. et al. Crumbling reefs and cold-water coral habitat loss in a future ocean: Evidence of "coralporosis" as an indicator of habitat integrity. *Front. Marine Sci.* **7**. https://doi.org/10.3389/fmars.2020.00668 (2020).
34. Woodall, L. C. et al. The deep sea is a major sink for microplastic debris. *R. Soc. Open Sci.* **1**, 140317–140317 (2014).
35. Freiwald, A., Fossa, J. H., Grehan, A., Koslow, T. & Roberts, J. M. *Cold-Water Coral Reefs: Out of Sight-no Longer Out of Mind*. 1–84 (Cambridge, UK, 2004).
36. Roberts, J. M., Wheeler, A. J. & Freiwald, A. Reefs of the deep: the biology and geology of cold-water coral ecosystems. *Science* **312**, 543–547 (2006).
37. Balogh, V., Fragkopoulou, E., Serrão, E. A. & Assis, J. A dataset of cold-water coral distribution records. *Data Brief.* **48**, 109223–109223 (2023).
38. Buhl-Mortensen, L., Olafsdottir, S. H., Buhl-Mortensen, P., Burgos, J. M. & Ragnarsson, S. A. Distribution of nine cold-water coral species (Scleractinia and Gorgonacea) in the cold temperate North

Atlantic: effects of bathymetry and hydrography. *Hydrobiologia* **759**, 39–61 (2015).
39. Keller, N. B. The deep-sea Madreporarian corals of the genus *Fungiacyathus* from the Kurile-Kamchatka, Aleutian Trenches and other regions of the world oceans. *Tr. Inst. Okeanologii* **99**, 31–44 (1976).
40. Roder, C. et al. First biological measurements of deep-sea corals from the Red Sea. *Sci. Rep.* **3**. https://doi.org/10.1038/srep02802. (2013)
41. Purkis, S. J. et al. Discovery of the deep-sea NEOM Brine Pools in the Gulf of Aqaba, Red Sea. *Commun. Earth Environ.* **3**. https://doi.org/10.1038/s43247-022-00482-x (2022).
42. Chimienti, G. et al. A new species of *Bathypathes* (Cnidaria, Anthozoa, Antipatharia, Schizopathidae) from the Red Sea and its phylogenetic position. *Zookeys* **1116**, 1–22 (2022).
43. Marenzeller, E. V. Expedition SM Schiff 'Pola' in das Rote Meer, nördliche und südliche Hälfte 1895 *Mathematisch-Naturwissenschaftliche Klasse* (1907).
44. Qurban, M. A. et al. Discovery of deep-water coral frameworks in the northern Red Sea waters of Saudi Arabia. *Sci. Rep.* **10**, 1–8 (2020).
45. Qurban, M. A. et al. In-situ observation of deep water corals in the northern Red Sea waters of Saudi Arabia. *Deep Sea Res. Part I: Oceanogr. Res. Pap.* **89**, 35–43 (2014).
46. Taviani, M., Correa, M. L. & Montagna, P. Last glacial deep-water corals from the Red Sea. *Bull. Mar. Sci.* **81**, 361–370 (2007).
47. Goreau, T. F. Calcium carbonate deposition by coralline algae and corals in relation to their roles as reef-builders. *Ann. N. Y. Acad. Sci.* **109**, 127–167 (1963).
48. Lombardi, C., Paul, D. T. & Silvia, C. *The Mediterranean Sea: Its History and Present Challenges.* 373–384 (Springer Science and Business Media, 2014).
49. Fagerstrom, J. A. Reef-building guilds and a checklist for determining guild membership: a new approach for study of communities. *Coral Reefs* **10**, 47–52 (1991).
50. Maier, S. R. et al. Reef communities associated with 'dead' cold-water coral framework drive resource retention and recycling in the deep sea. *Deep Sea Res. Part I Oceanogr. Res. Pap.* **175**. https://doi.org/10.1016/j.dsr.2021.103574 (2021).
51. Maggioni, D. et al. The first deep-sea Stylasterid (Hydrozoa, Stylasteridae) of the Red Sea. *Diversity* **14**, 241–241 (2022).
52. Meesters, E. et al. Sub-rubble communities of Curaçao and Bonaire coral reefs. *Coral Reefs* **10**, 189–197 (1991).
53. Raes, M. & Vanreusel, A. The metazoan meiofauna associated with a cold-water coral degradation zone in the Porcupine Seabight (NE Atlantic). *Cold-Water Corals Ecosyst*. 821–847. https://doi.org/10.1007/3-540-27673-4_43 (2005)
54. Davies, A. J., Roberts, J. M. & Hall-Spencer, J. Preserving deep-sea natural heritage: Emerging issues in offshore conservation and management. *Biol. Conserv.* **138**, 299–312 (2007).
55. Roberts, J. M., Henry, L. A., Long, D. & Hartley, J. P. Cold-water coral reef frameworks, megafaunal communities and evidence for coral carbonate mounds on the Hatton Bank, north east Atlantic. **54**, 297–316 (2008).
56. Anderson, O. F. et al. Habitat suitability models for predicting the occurrence of vulnerable marine ecosystems in the seas around New Zealand. *Deep-Sea Res. Part I Oceanogr. Res. Pap.* **115**, 265–292 (2016).
57. Hirzel, A. H. & Le Lay, G. Habitat suitability modelling and niche theory. *J. Appl. Ecol.* **45**, 1372–1381 (2008).
58. Duflot, R., Avon, C., Roche, P. & Bergès, L. Combining habitat suitability models and spatial graphs for more effective landscape conservation planning: an applied methodological framework and a species case study. *J. Nat. Conserv.* **46**, 38–47 (2018).
59. Wright, P. G. R., Coomber, F. G., Bellamy, C. C., Perkins, S. E. & Mathews, F. Predicting hedgehog mortality risks on British roads using habitat suitability modelling. *PeerJ* **2020**, e8154–e8154 (2020).
60. Martin, C. S. et al. Coralligenous and maërl habitats: Predictive modelling to identify their spatial distributions across the Mediterranean sea. *Sci. Rep.* **4**. https://doi.org/10.1038/srep05073 (2014).
61. Rowlands, G., Purkis, S. & Bruckner, A. Diversity in the geomorphology of shallow-water carbonate depositional systems in the Saudi Arabian Red Sea. *Geomorphology* **222**, 3–13 (2014).
62. Georgian, S. E., Anderson, O. F. & Rowden, A. A. Ensemble habitat suitability modeling of vulnerable marine ecosystem indicator taxa to inform deep-sea fisheries management in the South Pacific Ocean. *Fish. Res.* **211**, 256–274 (2019).
63. Rengstorf, A. M., Yesson, C., Brown, C. & Grehan, A. J. High-resolution habitat suitability modelling can improve conservation of vulnerable marine ecosystems in the deep sea. *J. Biogeogr.* **40**, 1702–1714 (2013).
64. Elith, J. et al. A statistical explanation of MaxEnt for ecologists. *Divers. Distrib.* **17**, 43–57 (2011).
65. Phillips, S. J., Dudik, M. & Schapire, R. E. A maximum entropy approach to species distrbution modeling. In *Proc. Twenty-first International Conference on Machine Learning*. 83 (2004).
66. Merow, C., Smith, M. J. & Silander, J. A. A practical guide to MaxEnt for modeling species' distributions: What it does, and why inputs and settings matter. *Ecography* **36**, 1058–1069 (2013).
67. Elith, J. & Graham, C. H. Do they? How do they? WHY do they differ? on finding reasons for differing performances of species distribution models. *Ecography* **32**, 66–77 (2009).
68. Elith, J. et al. Novel methods improve prediction of species' distributions from occurrence data. *Ecography* **29**, 129–151 (2006).
69. Piechaud, N., Downie, A., Stewart, H. A. & Howell, K. L. The impact of modelling method selection on predicted extent and distribution of deep-sea benthic assemblages. *Earth Environ. Sci. Trans. R. Soc. Edinb.* **105**, 251–261 (2015).
70. Préau, C., Bertrand, R. & Isselin-Nondedeu, F. Modeling potential distributions of three European amphibian species comparing ENFA and MaxEnt. *Herpetol. Conserv. Biol.* **13**, 91–104 (2018).
71. Scheer, G. & Pillai, C. S. *Report on the Stony Corals from the Red Sea*. Vol. 133 (Zoologica, 1983).
72. Rowlands, G., Purkis, S. & Bruckner, A. Tight coupling between coral reef morphology and mapped resilience in the Red Sea. *Mar. Pollut. Bull.* **105**, 575–585 (2016).
73. Burgos, J. M. et al. Predicting the Distribution of indicator taxa of vulnerable marine ecosystems in the arctic and sub-arctic waters of the Nordic Seas. *Front. Mar. Sci.* **7**. https://doi.org/10.3389/fmars.2020.00131 (2020).
74. Lobo, J. M., Jiménez-valverde, A. & Real, R. AUC: a misleading measure of the performance of predictive distribution models. *Glob. Ecol. Biogeogr.* **17**, 145–151 (2008).
75. Story, M. & Congalton, R. G. Accuracy assessment: a user's perspective. *Photogrammetric Eng. Remote Sens.* **52**, 397–399 (1986).
76. Warren, D. L. & Seifert, S. N. Ecological niche modeling in Maxent: the importance of model complexity and the performance of model selection criteria. *Ecol. Appl.* **21**, 335–342 (2011).
77. Fricke, H. W. & Hottinger, L. Coral bioherms below the euphotic zone in the Red sea. *Mar. Ecol. Prog. Ser.* **11**, 113–117 (1983).
78. Fricke, H. W. & Schuhmacher, H. The depth limits of Red Sea stony corals: An ecophysiological problem (a deep diving survey by submersible). *Mar. Ecol.* **4**, 163–194 (1983).
79. Gonzalez-Mirelis, G. & Buhl-Mortensen, P. Modelling benthic habitats and biotopes off the coast of Norway to support spatial management. *Ecol. Inform.* **30**, 284–292 (2015).
80. Tulloch, A. I. T. et al. Conservation planners tend to ignore improved accuracy of modelled species distributions to focus on multiple

threats and ecological processes. *Biol. Conserv.* **199**, 157–171 (2016).
81. Allen Coral Atlas. Imagery, maps and monitoring of the world's tropical coral reefs. (2022). https://doi.org/10.5281/zenodo.3833242
82. Freiwald, A. *Cold-Water Corals and Ecosystems*. Vol. 643 (Springer Science & Business Media, 2005).
83. Davies, A. J. & Guinotte, J. M. Global habitat suitability for framework-forming cold-water corals. *PLoS ONE* **6** https://doi.org/10.1371/journal.pone.0018483 (2011)
84. Mortensen, P. B. & Buhl-Mortensen, L. Morphology and growth of the deep-water gorgonians Primnoa resedaeformis and Paragorgia arborea. *Mar. Biol.* **147**, 775–788 (2005).
85. Sanna, G., Büscher, J. V. & Freiwald, A. Cold-water coral framework architecture is selectively shaped by bottom current flow. *Coral Reefs* **42**, 483–495 (2023).
86. Howell, K. L., Holt, R., Endrino, I. P. & Stewart, H. When the species is also a habitat: Comparing the predictively modelled distributions of *Lophelia pertusa* and the reef habitat it forms. *Biol. Conserv.* **144**, 2656–2665 (2011).
87. Benzoni, F., Bianchi, C. N. & Morri, C. Coral communities of the northwestern Gulf of Aden (Yemen): variation in framework building related to environmental factors and biotic conditions. *Coral Reefs* **22**, 475–484 (2003).
88. van der Kaaden, A. S. et al. Feedbacks between hydrodynamics and cold-water coral mound development. *Deep Sea Res. Part I: Oceanogr. Res. Pap.* **178**, 103641–103641 (2021).
89. Weinstein, D. K. et al. Mesophotic reef geomorphology categorization, habitat identification, and relationships with surface cover and terrace formation in the Gulf of Aqaba. *Geomorphology* **379**. https://doi.org/10.1016/j.geomorph.2020.107548. (2021)
90. Biton, E. & Gildor, H. The general circulation of the Gulf of Aqaba (Gulf of Eilat) revisited: The interplay between the exchange flow through the Straits of Tiran and surface fluxes. *J. Geophys. Res. Oceans* **116**, 8020–8020 (2011).
91. Pearman, T. R. R. et al. Improving the predictive capability of benthic species distribution models by incorporating oceanographic data—towards holistic ecological modelling of a submarine canyon. *Prog. Oceanogr.* **184**, 102338–102338 (2020).
92. Eyal, G. et al. *Euphyllia paradivisa*, a successful mesophotic coral in the northern Gulf of Eilat/Aqaba, Red Sea. *Coral Reefs* **35**, 91–102 (2016).
93. Tamir, R., Eyal, G., Kramer, N., Laverick, J. H. & Loya, Y. Light environment drives the shallow-to-mesophotic coral community transition. *Ecosphere* **10**. https://doi.org/10.1002/ecs2.2839. (2019).
94. Reijmer, J. J. G. Marine carbonate factories: review and update. *Sedimentology* **68**, 1729–1796 (2021).
95. Bracchi, V. A. et al. Mesophotic foraminiferal-algal nodules play a role in the Red Sea carbonate budget. *Commun. Earth Environ.* **4**, 288–288 (2023).
96. Heiss, G. A. Carbonate production by scleractinian corals at Aqaba, Gulf of Aqaba, Red Sea. *Facies* **33**, 19–34 (1995).
97. Serrano, O., Almahasheer, H., Duarte, C. M. & Irigoien, X. Carbon stocks and accumulation rates in Red Sea seagrass meadows. *Sci. Rep.* **8**. https://doi.org/10.1038/s41598-018-33182-8 (2018).
98. Purkis, S. J., Harris, P. M. & Ellis, J. Patterns of sedimentation in the contemporary Red Sea as an analog for ancient carbonates in rift settings. *J. Sediment. Res.* **82**, 859–870 (2012).
99. Kahng, S. E. et al. *Mesophotic Coral Ecosystems.* 801–828 (Springer, 2019).
100. Dullo, W.-C. et al. Holocene reef growth and recent carbonate production in the Red Sea. *Biogenic Sediment. I. Reef Evol. Res. Rep. Gettinger Arb. Geol. Palaont* **2**, 13–17 (1996).
101. Purkis, S. J., Rowlands, G. P., Riegl, B. M. & Renaud, P. G. The paradox of tropical karst morphology in the coral reefs of the arid Middle East. *Geology* **38**, 227–230 (2010).
102. Orejas, C. et al. Long-term growth rates of four Mediterranean cold-water coral species maintained in aquaria. *Mar. Ecol. Prog. Ser.* **429**, 57–65 (2011).
103. Ware, J. R., Smith, S. V. & Reaka-Kudla, M. L. Coral Reefs: Sources or sinks of atmospheric CO_2. *Coral Reefs* 127–130 (1991).
104. Nugraha, W. A. & Insafitri, I. Reefs as net carbon sources or net carbon sink? In *The 4th International Conference on Life Science and Technology (ICoLiST)* (2023).
105. Dullo, W. C. Coral growth and reef growth: a brief review. *Facies* **51**, 33–48 (2005).
106. Roff, G. Reef accretion and coral growth rates are decoupled in Holocene reef frameworks. *Marine Geol.* **419**. https://doi.org/10.1016/j.margeo.2019.106065 (2020).
107. Gardiner, J. S. & Waugh, P. *Madreporaria Excluding Flabellidae and Turbinolidae*. order of the Trustees of the British Museum (London, 1939).
108. Cairns, S. D. *A Generic Revision and Phylogenetic Analysis of the Dendrophylliidae (Cnidaria: Scleractinia)*. Smithsonia Contributions to Zoology (2001).
109. Sappington, J. M., Longshore, K. M. & Thompson, D. B. Quantifying landscape ruggedness for animal habitat analysis: a case study using bighorn sheep in the Mojave Desert. *J. Wildl. Manag.* **71**, 1419–1426 (2007).
110. Purkis, S. J. & Kohler, K. E. The role of topography in promoting fractal patchiness in a carbonate shelf landscape. *Coral Reefs* **27**, 977–989 (2008).
111. Mohn, C. et al. Linking benthic hydrodynamics and cold-water coral occurrences: a high-resolution model study at three cold-water coral provinces in the NE Atlantic. *Prog. Oceanogr.* **122**, 92–104 (2014).
112. Moreno Navas, J. et al. Ecohydrodynamics of cold-water coral reefs: a case study of the Mingulay Reef Complex (Western Scotland). *PLoS ONE* **9**, e98218 (2014).
113. Iwahashi, J. & Pike, R. J. Automated classifications of topography from DEMs by an unsupervised nested-means algorithm and a three-part geometric signature. *Geomorphology* **86**, 409–440 (2007).
114. Gullage, L., Devillers, R. & Edinger, E. Predictive distribution modelling of cold-water corals in the Newfoundland and Labrador region. *Mar. Ecol. Prog. Ser.* **582**, 57–77 (2017).
115. Kinlan, B. P. et al. Predictive modeling of suitable habitat for deep-sea corals offshore the Northeast United States. *Deep-Sea Res. Part I: Oceanogr. Res. Papers* **158**. https://doi.org/10.1016/j.dsr.2020.103229 (2020).
116. Morales, N. S., Fernández, I. C. & Baca-González, V. MaxEnt's parameter configuration and small samples: are we paying attention to recommendations? A systematic review. *PeerJ* **5**, e3093–e3093 (2017).
117. Berumen, M. L. et al. *Fishes and Connectivity of Red Sea Coral Reefs*. 157–179. (Springer, 2019)
118. Larsson, A. I. & Purser, A. Sedimentation on the cold-water coral *Lophelia pertusa*: Cleaning efficiency from natural sediments and drill cuttings. *Mar. Pollut. Bull.* **62**, 1159–1168 (2011).
119. Ross, R. E. & Howell, K. L. Use of predictive habitat modelling to assess the distribution and extent of the current protection of 'listed' deep-sea habitats. *Divers. Distrib.* **19**, 433–445 (2013).
120. Röthig, T., Yum, L. K., Kremb, S. G., Roik, A. & Voolstra, C. R. Microbial community composition of deep-sea corals from the Red Sea provides insight into functional adaption to a unique environment. *Nat. Publ. Group*. https://doi.org/10.1038/srep44714. (2017)
121. Pike, R. J., Evans, I. S. & Hengl, T. *Geomorphometry: A Brief Guide*. Vol. 33 (Elsevier Ltd, 2009).
122. Conrad, O. et al. System for Automated Geoscientific Analyses (SAGA) v. 2.1.4. *Geosci. Model Dev.* **8**, 1991–2007 (2015).

123. Dolan, M. F. J., Grehan, A. J., Guinan, J. C. & Brown, C. Modelling the local distribution of cold-water corals in relation to bathymetric variables: Adding spatial context to deep-sea video data. *Deep-Sea Res. Part I: Oceanogr. Res. Pap.* **55**, 1564–1579 (2008).
124. Schlitzer, Reiner, Ocean Data View, odv.awi.de (2023).
125. Sapna, K., Thangavelu, A., Mithran, S. & Shanthi, K. Spatial analysis of river water quality using inverse distance weighted interpolation in Noyyal watershed in Coimbatore, Tamilnadu, India. *Res. J. Life Sci. Bioinform. Pharmaceut. Chem. Sci.* **4**. https://doi.org/10.26479/2018.0401.13. (2018)
126. Tyberghein, L. et al. Bio-ORACLE: a global environmental dataset for marine species distribution modelling. *Glob. Ecol. Biogeogr.* **21**, 272–281 (2012).
127. Gardiner, J. S. & Waugh, P. *The Flabellid and Turbinolid Corals*. (London, 1938).
128. R Foundation for Statistical Computing. *A Language and Environment for Statistical Computing* (R Foundation for Statistical Computing, Vienna, Austria, 2020).
129. Tong, R., Purser, A., Guinan, J. & Unnithan, V. Modeling the habitat suitability for deep-water gorgonian corals based on terrain variables. *Ecol. Inform.* **13**, 123–132 (2013).
130. Phillips, S. J. & Dudík, M. Modeling of species distributions with Maxent: new extensions and a comprehensive evaluation. *Ecography* **31**, 161–175 (2008).
131. Peterson, E. A. et al. Graph-theoretic modeling reveals connectivity hotspots for herbivorous reef fishes in a restored tropical island system. *Landsc. Ecol.* **39**, 145 (2024).
132. Hao, T., Elith, J., Lahoz-Monfort, J. J. & Guillera-Arroita, G. Testing whether ensemble modelling is advantageous for maximising predictive performance of species distribution models. *Ecography* **43**, 549–558 (2020).
133. Brotons, L., Thuiller, W., Araújo, M. B. & Hirzel, A. H. Presence-absence versus presence-only modelling methods for predicting bird habitat suitability. *Ecography* **27**, 437–448 (2004).
134. MacKenzie, D. I. et al. Estimating site occupancy rates when detection probabilities are less than one. *Ecology* **83**, 2248–2255 (2002).
135. Muscarella, R. et al. ENMeval: an R package for conducting spatially independent evaluations and estimating optimal model complexity for Maxent ecological niche models. *Methods Ecol. Evol.* **5**, 1198–1205 (2014).
136. Allouche, O., Tsoar, A. & Kadmon, R. Assessing the accuracy of species distribution models: prevalence, kappa and the true skill statistic (TSS). *J. Appl. Ecol.* **43**, 1223–1232 (2006).
137. Liu, C., Newell, G. & White, M. On the selection of thresholds for predicting species occurrence with presence-only data. *Ecol. Evol.* **6**, 337–348 (2016).
138. Yum, L. K. et al. Transcriptomes and expression profiling of deep-sea corals from the Red Sea provide insight into the biology of azooxanthellate corals. *Sci. Rep.* **7**. https://doi.org/10.1038/s41598-017-05572-x. (2017).
139. Hodgson, G. Sediment and the settlement of larvae of the reef coral *Pocillopora damicornis*. *Coral Reefs* **9**, 41–43 (1990).
140. Wilson, M. F. J., O'Connell, B., Brown, C., Guinan, J. C. & Grehan, A. J. Multiscale terrain analysis of multibeam bathymetry data for habitat mapping on the continental slope. *Mar. Geod.* **30**, 3–35 (2007).
141. Haas, A. F., Smith, J. E., Thompson, M. & Deheyn, D. D. Effects of reduced dissolved oxygen concentrations on physiology and fluorescence of hermatypic corals and benthic algae. *PeerJ* **2014**. https://doi.org/10.7717/peerj.235 (2014).
142. Ding, D. S., Patel, A. K., Singhania, R. R., Chen, C. W. & Dong, C. D. Effects of temperature and salinity on growth, metabolism and digestive enzymes synthesis of Goniopora columna. *Biology* **11**. https://doi.org/10.3390/biology11030436 (2022).
143. Brooke, S., Ross, S. W., Bane, J. M., Seim, H. E. & Young, C. M. Temperature tolerance of the deep-sea coral *Lophelia pertusa* from the southeastern United States. *Deep-Sea Res. Part II: Topical Stud. Oceanogr.* **92**, 240–248 (2013).

Acknowledgements

This research was undertaken in accordance with the policies and procedures of the King Abdullah University of Science and Technology (KAUST). Permission relevant for KAUST to undertake the research was obtained from the applicable governmental agencies in the Kingdom of Saudi Arabia. We would like to thank NEOM for the organisation and facilitation of the Red Sea Deep Blue expedition, as well as A.A.E. and Paul Marshall for their logistical support. We extend our gratitude to the entire crew of OceanXplorer, and in particular, we wish to acknowledge the ROV team, led by Andrew Craig, and the submersible team, led by Mark Taylor, for the acquisition of scientific data. This research was supported by KAUST (funding code FCC/1/1973-50-01 and baseline research funds to F.B.).

Author contributions

M.K.B.N., F.M., S.J.P. and F.B. conceived the research and designed the methodology. M.K.B.N. generated the models and conducted a formal analysis. F.M., S.J.P., M.O., T.I.T., G.C., M.R. and F.B. contributed to fieldwork and original data acquisition. M.K.B.N. wrote the original draft, and F.M., S.J.P., M.O., M.K., T.I.T., G.C. and F.B. contributed to the review and editing of the manuscript. A.A.E. was the expedition leader of the 2020 Deep Blue Expedition. Project administration was done by M.R., A.A.E., B.J. and F.B., and supervision was done by F.M. and F.B.

Competing interests

The authors declare no competing interests.

Additional information

Supplementary information The online version contains supplementary material available at https://doi.org/10.1038/s43247-024-01830-9.

Correspondence and requests for materials should be addressed to Megan K. B. Nolan.

Peer review information *Communications Earth & Environment* thanks Peter Etnoyer and the other, anonymous, reviewer(s) for their contribution to the peer review of this work. Primary handling editors: Alice Drinkwater. [A peer review file is available.].